arXiv:2608.24891v1 [cs.AI] 1 Jun 2026

Measurement-Budget Allocation in Quantum Learning with Finite-Shot Generalization Guarantees

Ferhat Ozgur Catak
Department of Electrical Engineering and Computer Science
University of Stavanger, Norway
f.ozgur.catak@uis.no

August 27, 2026

Abstract

On near-term quantum hardware, estimating a Born probability requires repeated circuit executions. A quantum learning experiment with a fixed measurement budget B must therefore decide how many distinct training states n to use and how many shots S to allocate to each state. We study this tradeoff for binary quantum classifiers with fixed or independently selected measurement operators M, where the ideal score is $\mathrm{Tr}(M\rho)$. We prove a distribution-free generalization bound that separates the finite-sample and finite-shot contributions. The sample term scales as $\sqrt{d/n}$, while the shot term scales as $\sqrt{(\log n)/S}$; under the constraint $B = nS$, these two terms move in opposite directions. Minimising a conservative closed-form surrogate of the bound gives the allocation rule $n^* = 2\sqrt{2dB/\log(2B/\delta)}$ and $S^* = B/n^*$. This surrogate has the same asymptotic scaling as the exact minimizer and yields a worst-case rate of $B^{-1/4}$. The guarantee is intentionally conservative, since it applies to the full class of binary quantum measurements. We complement the theory with PennyLane simulations using 2-qubit and 4-qubit variational quantum circuits on nine synthetic binary classification benchmarks. In all tested configurations, the one-sided empirical generalization gap remains below the theoretical bound. The result provides a conservative statistical guideline for allocating measurement budgets in finite-shot evaluation and pre-experimental planning for near-term quantum learning systems, complementing hardware-level scheduling and circuit-design considerations. Extending the guarantee to fully adaptive shot-noisy training remains an open problem.

Keywords: quantum machine learning, measurement budget allocation, finite-shot generalization bounds, Rademacher complexity, NISQ devices, resource planning.

1 Introduction

Near-term quantum devices are subject to constraints that do not arise in the same form on classical computing platforms [1–3]. Gate times, coherence limits, and access restrictions on cloud-based quantum processors all limit the number of circuit executions available for a given experiment. For quantum learning, a particularly important constraint is the *shot cost*: the number of repeated circuit executions required to estimate the expectation value of a measurement.

A quantum classifier assigns a score to a quantum state ρ through a measurement operator M. The ideal score is the Born probability

$$p_M(\rho) = \mathrm{Tr}(M\rho) \in [0, 1].$$

This quantity is not observed directly. Instead, each circuit execution produces a binary outcome $Z \in 0, 1$ with $\Pr(Z = 1) = \mathrm{Tr}(M\rho)$, and the probability must be estimated from repeated

measurements. Estimating $\mathrm{Tr}(M\rho)$ to accuracy ε requires on the order of $1/(4\varepsilon^2)$ independent shots. Thus, shot cost is not merely an implementation detail, but a statistical constraint imposed by the measurement process itself. Recent work on quantum neural networks and quantum learning has also emphasized that finite sampling noise is a fundamental statistical effect, even on otherwise ideal quantum devices, because expectation-value outputs must be estimated from repeated measurements [4, 5].

Shots should therefore be treated as a statistical resource in their own right, separate from the number of training states. In a typical quantum learning experiment, the total measurement budget is

$$B = n \times S,$$

where n denotes the number of distinct training states and S the number of shots assigned to each state. Standard statistical learning theory does not directly address how such a budget should be divided between these two quantities. It usually treats the number of training examples as the only statistical resource and assumes exact access to hypothesis evaluations, whereas finite-shot quantum experiments provide only noisy estimates of Born probabilities.

In many quantum machine learning studies, the common choice is to use a relatively large number of shots and a small number of training states [6–9]. This is understandable, partly because quantum circuit simulation is expensive and repeated measurements are often used to stabilise estimates. However, this choice is not usually derived from a statistical allocation principle. Under a fixed total budget B, it can place the experiment in a sample-limited regime, where increasing the number of training states would reduce the generalization error more effectively than the corresponding decrease in shots would increase the estimation error.

The central question is therefore how to allocate a fixed budget $B = nS$ between n and S. A useful allocation must balance two sources of error: the error due to observing only finitely many training states, and the error due to estimating each quantum score from finitely many measurement outcomes.

Many training states, few shots per state. If n is increased while the total budget B is fixed, then $S = B/n$ decreases. Each estimate $\hat{p}_{M,S}(\rho_i)$ is then based on fewer measurement outcomes and becomes less reliable. In the limiting case $S = 1$, the estimate is a single Bernoulli outcome with variance at most $1/4$, so the observed training scores carry substantial measurement noise.

Few training states, many shots per state. If S is increased under the same fixed budget, then $n = B/S$ decreases. The Born probabilities are estimated more accurately, but the learner observes fewer distinct training states. In the limiting case $n = 1$, shot noise can be made small, but the finite-sample component of the generalization gap remains of order $O(1)$.

A useful allocation must therefore lie between these two regimes. Its position depends on the Hilbert-space dimension $d = 2^k$ for k qubits, the total budget B, and the confidence level δ. The analysis below derives a closed-form surrogate allocation rule from a finite-shot generalization bound.

One might try to analyse the shot-estimated empirical risk using standard generalization theory. However, this does not by itself resolve the allocation problem.

The first difficulty is that the observed score $\hat{p}_{M,S}(\rho_i)$ is only an estimate of the Born probability $p_M(\rho_i) = \mathrm{Tr}(M\rho_i)$. Classical bounds usually assume that hypothesis values are evaluated exactly. In the finite-shot setting, the empirical loss is computed from noisy measurement estimates, and the size of this perturbation depends explicitly on S.

The second difficulty is that classical learning theory treats the number of training examples n as the main statistical resource. It does not provide a rule for choosing both n and S under the constraint $nS = B$. Existing quantum generalization bounds [10, 11] either work in the infinite-shot regime or keep the number of shots fixed. They therefore do not directly address how a finite measurement budget should be split between additional training states and more

accurate measurement estimates. We address this issue by incorporating finite-shot noise into a Rademacher-complexity analysis.

We adapt the Rademacher-complexity framework [12] to account for finite-shot quantum measurements. The first part of the analysis concerns the ideal, infinite-shot setting. For the measurement class

$$\mathcal{H}_{\mathrm{POVM}} = M : 0 \leq M \leq I,$$

we show that

$$\hat{\mathcal{R}}_n^{(\infty)}(\mathcal{H}_{\mathrm{POVM}}) \leq \sqrt{d/n}.$$

The proof uses the linearity of $\mathrm{Tr}(M\cdot)$ and the fact that, for a fixed Hermitian matrix, the optimizing measurement is the projector onto its positive eigenspace. Standard nuclear- and Frobenius-norm bounds then give the stated dependence on the Hilbert-space dimension d and the number of training states n.

The second part of the analysis accounts for finite measurement shots. We bound the deviation between the ideal empirical risk and the shot-estimated empirical risk using Hoeffding concentration together with the Lipschitz property of the loss. Combining the sample and shot deviations yields a bound with two separate contributions: a finite-sample term controlled by n, and a finite-shot term controlled by S. Under the budget constraint $B = nS$, these terms lead to a closed-form surrogate allocation rule for choosing n and S.

The resulting generalization bound has the structure:

$$\underbrace{R_\ell(M)}_{\text{population risk}} \leq \underbrace{\hat{R}_{n,S,\ell}(M)}_{\text{observed empirical risk}} + \underbrace{2L\sqrt{\frac{d}{n}}}_{\substack{\text{sample term}\\ \text{(classical)}}} + \underbrace{L\sqrt{\frac{\log(4n/\delta)}{2S}}}_{\substack{\text{shot term}\\ \text{(quantum-native)}}} + \underbrace{\sqrt{\frac{\log(2/\delta)}{2n}}}_{\substack{\text{confidence}\\ \text{term}}} \tag{1}$$

Substituting $S = B/n$ makes the two terms move in opposite directions: the sample term decreases with n, while the shot term increases as fewer shots are assigned to each state. This gives a U-shaped upper bound as a function of n. To obtain a closed-form planning rule, we use the conservative replacement $\log(2n/\delta) \leq \log(2B/\delta)$ for $n \leq B$. Minimising the resulting surrogate bound gives

$$n^* = 2\sqrt{\frac{2dB}{\log(2B/\delta)}}, \qquad S^* = \frac{B}{n^*} = \frac{1}{2}\sqrt{\frac{B\log(2B/\delta)}{2d}} \tag{2}$$

Both n^* and S^* scale as $\sqrt{B/\log B}$. At this surrogate allocation the worst-case bound decays at rate:

$$\mathcal{G}(n^*) = O\left(\left(\frac{d\log B}{B}\right)^{1/4}\right) \tag{3}$$

The rate $B^{-1/4}$ is slower than the classical $B^{-1/2}$ rate, but the two rates are not measured against the same resource unit. In the quantum setting, B counts individual binary measurement outcomes. In classical learning, a training example is usually treated as a complete labelled observation. The slower rate therefore reflects the way the measurement budget is counted, rather than a fundamental inefficiency of quantum learning.

For readers acquainted with classical learning theory, several structural parallels clarify the quantum setting.

The measurement class $\mathcal{H}_{\mathrm{POVM}} = M : 0 \leq M \leq I$ plays a role similar to bounded linear classifiers of the form $x \mapsto \langle w, x\rangle : |w| \leq \Lambda$. In both cases, the hypothesis is specified by a constrained linear functional, and the corresponding Rademacher complexity scales as $O(1/\sqrt{n})$, up to dimension-dependent factors. The quantum case differs in one essential respect: the value

$\mathrm{Tr}(M\rho)$ is not directly observed, but estimated from binary measurement outcomes, while $\langle w, x_i \rangle$ is available exactly in the classical setting.

Shot noise can be viewed as a measurement-induced analogue of noise in the empirical loss. Its size decreases with the number of shots, typically at order $O(1/\sqrt{S})$. Unlike ordinary label noise, however, shot noise is not fixed by the data-generating process. It is partly controlled by the experimental design, since the practitioner chooses how many shots S to allocate to each state.

The rate $B^{-1/4}$ also has an interpretation in terms of resource splitting. A fixed budget must be divided between observing more training states and estimating each quantum score more accurately. Optimising these two objectives jointly leads to a slower rate than optimising either one in isolation. This should be understood as a consequence of the budget model, where B counts individual measurement outcomes, rather than as a fundamental limitation of quantum learning.

The guarantee has the same distribution-free character as classical Rademacher bounds. It applies to any distribution $\mathcal{P}$ over quantum states and labels, any L-Lipschitz loss, and any measurement $M \in \mathcal{H}_{\mathrm{POVM}}$ chosen independently of the shot outcomes used to compute the empirical risk.

Summary of contributions are as follows

C1. Finite-shot generalization bound. Theorem 3.1 gives a distribution-free bound (1) for quantum measurement hypotheses. The bound separates the finite-sample contribution, of order $O(\sqrt{d/n})$, from the finite-shot contribution, of order $O(\sqrt{(\log n)/S})$.

C2. Conservative allocation rule under a fixed measurement budget. Under the constraint $B = nS$, Theorem 3.2 derives a closed-form allocation rule for a conservative surrogate of the finite-shot evaluation bound:

$$n^* = 2\sqrt{\frac{2dB}{\log(2B/\delta)}}, \qquad S^* = \frac{B}{n^*}.$$

This rule minimizes the surrogate upper bound for fixed or independently selected measurements. It should therefore be interpreted as a planning baseline for finite-shot evaluation, rather than as an optimality guarantee for fully adaptive shot-noisy training.

C3. Sample-limited and shot-limited regimes. The analysis identifies three regimes: sample-limited, shot-limited, and balanced. These regimes clarify how the bound changes when budget is moved between additional training states and additional shots per state. They also explain why configurations with large S and small n, which are common in QML studies, may be sample-limited under a fixed budget.

C4. Empirical consistency checks. We test the bound using PennyLane simulations with 2-qubit ($d = 4$) and 4-qubit ($d = 16$) variational quantum circuits on nine synthetic binary classification benchmarks. Across the tested values of n, S, and B, the one-sided empirical generalization gaps remain below the theoretical bound. These experiments are used as consistency checks, not as evidence of tightness, since the tested VQCs form a restricted subclass of $\mathcal{H}_{\mathrm{POVM}}$ on structured data.

C5. Implications for experiment design. The allocation rule provides a conservative starting point for choosing n and S when evaluating fixed or independently selected quantum hypotheses under a finite measurement budget. For adaptive shot-noisy training, the same tradeoff is expected to be relevant, but the present theorem does not provide a complete training-time generalization guarantee.

The PennyLane-based experimental code and synthetic-dataset generation scripts supporting the findings of this study are publicly available at GitHub [1].

The remainder of the paper is structured as follows. Section 2 reviews related work. Section 3 introduces the system model, the two-gap decomposition, the main generalization bound in Theorem 3.1, its scope, and the surrogate allocation rule in Theorem 3.2. Section 4 presents the experimental results. Section 5 discusses implications, limitations, and open problems. Section 6 concludes the paper.

2 Related Work

We organise prior work around three capabilities that are required to answer the budget allocation question: (Q1) Does the framework account for finite measurement shots? (Q2) Does it jointly optimise n (training states) and S (shots per state)? (Q3) Does it yield a closed-form allocation rule for fixed budget $B = nS$? Table 1 summarises the comparison; the paragraphs below describe the focus of each prior approach and explain why the allocation question under finite B lies outside its scope.

Table 1: Comparison of quantum generalization frameworks along three axes relevant to the budget allocation problem. ✓ = addressed; × = not in scope; ∼ = partially.

Work	Method	(Q1) Finite shots?	(Q2) Joint n-S?	(Q3) Alloc. formu
Caro et al. [10]	Covering numbers	×	×	×
Haug & Kim [11]	Quantum Fisher info	×	×	×
Huang et al. [13]	Info-theoretic	×	×	×
Gil-Fuster et al. [14]	Expressibility	∼	×	×
Bshouty & Jackson [15]	Quantum PAC	×	×	×
This work	Rademacher complexity	✓	✓	✓

Covering numbers for parameterised quantum circuits [10]. Caro et al. derive generalization bounds of order $O(\sqrt{T/n})$ for parameterised quantum circuits with T trainable gates, via covering numbers in the infinite-shot limit ($S \to \infty$). This work is complementary to ours: it studies finite-sample generalization for PQC-induced function classes, whereas we study finite-shot corrections for the full measurement class $\mathcal{H}_{\mathrm{POVM}}$. The covering-number metric is defined on exact hypothesis values and does not extend to shot-estimated approximations, so the framework does not directly yield guidance on S or on the tradeoff under fixed B.

Quantum Fisher information [11]. Haug and Kim bound generalization error via the quantum Fisher information (QFI) metric evaluated at a fixed parameter point. QFI is a local quantity that characterises parameter-space sensitivity and is well suited to the study of trainability and barren plateaus. Because QFI is defined in the infinite-shot limit and provides a bound at a single parameter point rather than over the full class $\mathcal{H}_{\mathrm{POVM}}$, it does not yield allocation guidance for finite S. The two approaches are complementary: QFI bounds inform circuit design and optimisation, while the present bound informs measurement resource allocation.

Information-theoretic limits [13]. Huang, Kueng, and Preskill establish bounds on quantum advantage in terms of the number of training examples required. Their budget is a count of

[1] https://github.com/ocatak/quantum-measurement-budget-allocation

training examples; ours is a count of measurement outcomes. The two frameworks address complementary aspects of quantum learning complexity and are non-overlapping in scope.

Quantum PAC learning [15, 16]. The quantum PAC learning literature studies classical concept classes learned from quantum example oracles, where the quantum resource is the oracle access model. Our setting is structurally complementary: quantum hypothesis classes (measurement operators $M \in \mathcal{H}_{\text{POVM}}$) applied to quantum state data, with explicit finite-shot accounting. Neither framework subsumes the other.

Rethinking quantum generalization [14]. Gil-Fuster et al. raise important concerns about the direct transfer of classical capacity measures (VC dimension, covering numbers) to quantum models. The present work addresses one concrete instance of this challenge: the Rademacher complexity of the full measurement class $\mathcal{H}_{\text{POVM}}$ is $\sqrt{d/n}$ in the infinite-shot limit, and the additive shot-noise correction is $\sqrt{(\log n)/S}$. Rademacher complexity has also been used to quantify the statistical complexity of quantum circuits and parameterised quantum models, including encoding-dependent generalization bounds for PQCs and complexity analyses of noisy quantum circuits [17–19]. The present analysis differs by considering the full binary measurement class $\mathcal{H}_{\text{POVM}}$ and by adding an explicit finite-shot perturbation term.

Shadow tomography [20, 21]. The signed-average matrix $\bar{\rho}_\sigma = \frac{1}{n}\sum_i \sigma_i \rho_i$ arising in the Rademacher complexity proof is structurally related to the classical shadow estimators used in shadow tomography. Formalising this connection and determining whether shadow techniques could tighten the present bound is identified as an open problem in Section 5.

Classical-shadow methods show that, for suitable randomized measurement schemes, many linear properties of a quantum state can be predicted from surprisingly few measurements [21].

Summary. Prior work on quantum generalization predominantly studies the infinite-shot or fixed-shot regime and does not directly address the joint optimisation of n and S under a fixed total budget $B = nS$. The Rademacher complexity framework, with shot noise modelled as a Lipschitz perturbation of the empirical risk, makes this joint optimisation tractable and yields a closed-form allocation rule. The approaches are complementary rather than competing: covering-number and QFI analyses address circuit expressibility and optimisation, while the present work addresses measurement resource allocation.

3 System Model and Main Results

3.1 Quantum Learning Setup

Quantum training examples. A quantum training example is a pair (ρ_i, y_i) where ρ_i is a *density matrix*, a $d \times d$ positive semidefinite operator with unit trace and $y_i \in \{0, 1\}$ is its label. The training set $\mathcal{D} = \{(\rho_i, y_i)\}_{i=1}^n$ is drawn i.i.d. from an unknown distribution $\mathcal{P}$ over $\mathcal{S}(\mathcal{V}) \times \{0, 1\}$.

Quantum hypotheses. A quantum hypothesis is a measurement operator M with $0 \leq M \leq I$, where I is the $d \times d$ identity. Its prediction score on state ρ is the Born probability $p_M(\rho) = \text{Tr}(M\rho) \in [0, 1]$. The full binary measurement hypothesis class is:

$$\mathcal{H}_{\text{POVM}} = \{M : 0 \leq M \leq I,\ M \in \mathbb{C}^{d \times d}\}$$

For k qubits, $d = 2^k$.

Finite-shot estimation. Performing S independent applications of $\{M, I - M\}$ on state ρ_i produces outcomes $Z_{i,1}, \ldots, Z_{i,S} \in \{0, 1\}$. The shot-estimated score is:

$$\hat{p}_{M,S}(\rho_i) = \frac{1}{S} \sum_{s=1}^{S} Z_{i,s}, \qquad \mathbb{E}[\hat{p}_{M,S}(\rho_i)] = \mathrm{Tr}(M\rho_i), \qquad \mathrm{Var}[\hat{p}_{M,S}(\rho_i)] \leq \frac{1}{4S} \tag{4}$$

Loss function. We consider L-Lipschitz losses: $|\ell(p_1, y) - \ell(p_2, y)| \leq L|p_1 - p_2|$. The squared loss $(p - y)^2$ satisfies this with $L = 2$. The rescaled binary hinge loss used in Section 4 is bounded in $[0, 1]$ and satisfies the condition with $L = 1$. The hard-threshold $0/1$ loss is excluded because its discontinuity near the decision boundary makes the finite-shot analysis intractable without an additional margin assumption.

3.2 Three Layers of Statistical Error

The learning pipeline involves three risk quantities, listed in Table 2. Of these, only the shot-estimated empirical risk can be measured directly on a quantum device. The aim is therefore to control the population risk using this observable quantity.

Table 2: Three layers of statistical error in quantum learning.

Quantity	Symbol	Definition	Observable?
Population risk	$R_\ell(M)$	$\mathbb{E}_{(\rho,y)\sim\mathcal{P}}[\ell(p_M(\rho), y)]$	No — requires the full distribution
Ideal empirical risk	$\hat{R}_{n,\ell}(M)$	$\frac{1}{n}\sum_i \ell(p_M(\rho_i), y_i)$	No — requires infinite shots
Shot-estimated empirical risk	$\hat{R}_{n,S,\ell}(M)$	$\frac{1}{n}\sum_i \ell(\hat{p}_{M,S}(\rho_i), y_i)$	**Yes**

3.3 Two-Gap Structure and Main Bound

Figure 1 illustrates how the two statistical gaps arise in the quantum learning pipeline.

The capacity of $\mathcal{H}_{\mathrm{POVM}}$ under random labelling is characterised by the following result, proved in Appendix A.

Proposition 3.1. Capacity of the quantum measurement class

For $\mathcal{H}_{\mathrm{POVM}}$ on a d-dimensional Hilbert space and any n training states:

$$\hat{\mathcal{R}}_n^{(\infty)}(\mathcal{H}_{\mathrm{POVM}}) \leq \sqrt{\frac{d}{n}} \tag{5}$$

Proof sketch. For a fixed sign vector σ, define

$$\bar{\rho} * \sigma = \frac{1}{n} \sum_i \sigma_i \rho_i \tag{6}$$

By linearity of the trace, the supremum over M is an optimization over a Hermitian matrix. It is attained by projecting onto the positive eigenspace of $\bar{\rho} * \sigma$. Hence the supremum is bounded by $|\bar{\rho}_\sigma| * 1$. Using

$$|\bar{\rho} * \sigma| * 1 \leq \sqrt{d}, |\bar{\rho} * \sigma| * F \tag{7}$$

and the sign cancellation in the Rademacher average, together with $|\rho_i| * F \leq 1$, gives

$$\mathbb{E} * \sigma! \, [|\bar{\rho} * \sigma|_F] \leq \frac{1}{\sqrt{n}} \tag{8}$$

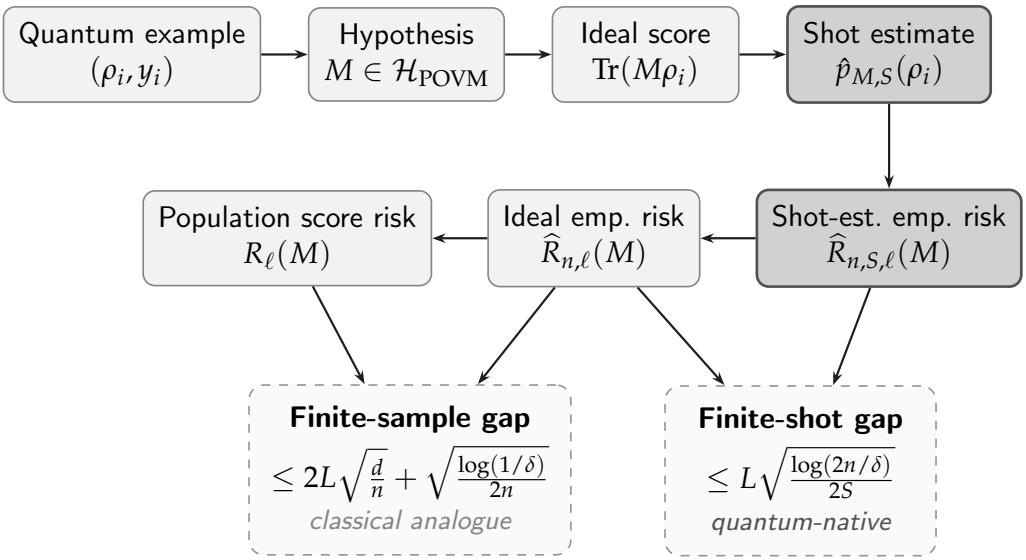

Theorem 3.1:

$$R_\ell(M) \;\leq\; \widehat{R}_{n,S,\ell}(M) \;+\; 2L\sqrt{\frac{d}{n}} \;+\; L\sqrt{\frac{\log(4n/\delta)}{2S}} \;+\; \sqrt{\frac{\log(2/\delta)}{2n}}$$

Figure 1: The quantum learning pipeline and its two sources of error. The finite-sample gap arises because the learner observes only n training states from the data distribution. The finite-shot gap arises because each score $\mathrm{Tr}(M\rho_i)$ is estimated from S binary measurement outcomes. Theorem 3.1 bounds the combined effect of these two errors.

This yields the stated bound; the full argument is given in Appendix A. □

Combining this capacity bound with Hoeffding concentration for the shot estimates gives the main theorem, proved in Appendix B.

Theorem 3.1. Generalization bound with finite shots

Let $M \in \mathcal{H}_{\mathrm{POVM}}$ be chosen independently of the shot outcomes used to compute $\hat{R}_{n,S,\ell}(M)$, and let $\ell : [0,1] \times \{0,1\} \to [0,1]$ be L-Lipschitz in its first argument. Then, with probability at least $1-\delta$ over the sample draw and the measurement outcomes,

$$\underbrace{R_\ell(M)}_{\text{population risk}} \;\leq\; \underbrace{\hat{R}_{n,S,\ell}(M)}_{\text{observed empirical risk}} \;+\; \underbrace{2L\sqrt{\frac{d}{n}}}_{\substack{\text{sample term}\\ \text{(classical)}}} \;+\; \underbrace{L\sqrt{\frac{\log(4n/\delta)}{2S}}}_{\substack{\text{shot term}\\ \text{(quantum-native)}}} + \underbrace{\sqrt{\frac{\log(2/\delta)}{2n}}}_{\substack{\text{confidence}\\ \text{term}}} \tag{9}$$

Scope of the finite-shot guarantee. Theorem 3.1 assumes that M is chosen independently of the measurement outcomes used to compute the observed empirical risk $\hat{R}_{n,S,\ell}(M)$. This setting covers, for example, the evaluation of a fixed trained hypothesis using a separate shot budget, as well as pre-experimental resource planning for a given measurement class. If the same shot-noisy losses are also used to select M, as in adaptive training, this independence no longer holds. In that case, additional uniform-convergence or algorithm-specific arguments are needed to control the dependence between the selected hypothesis and the measurement noise. Extending the analysis to fully adaptive shot-noisy training remains an open problem.

Table 3 contrasts the structure of the bound with its classical analogue.

Table 3: Structural comparison of classical and quantum generalization bounds.

Property	**Classical**	**Quantum (this work)**
Score observation	Direct	S binary shots (Born rule)
Sample error term	$O(1/\sqrt{n})$	$O(\sqrt{d/n})$
Shot error term	None	$O(\sqrt{(\log n)/S})$
Resources to plan	n only	n *and* S
Surrogate budget-rate scaling	$O(B^{-1/2})$	$O(B^{-1/4})$

3.4 Conservative Surrogate Budget Allocation

Substituting $S = B/n$ into (9) and dropping the confidence term yields a U-shaped function of n:

$$\mathcal{G}(n) = \underbrace{\frac{2\sqrt{d}}{\sqrt{n}}}_{f_1(n)\downarrow} + \underbrace{\sqrt{\frac{n\log(2n/\delta)}{2B}}}_{f_2(n)\uparrow} \tag{10}$$

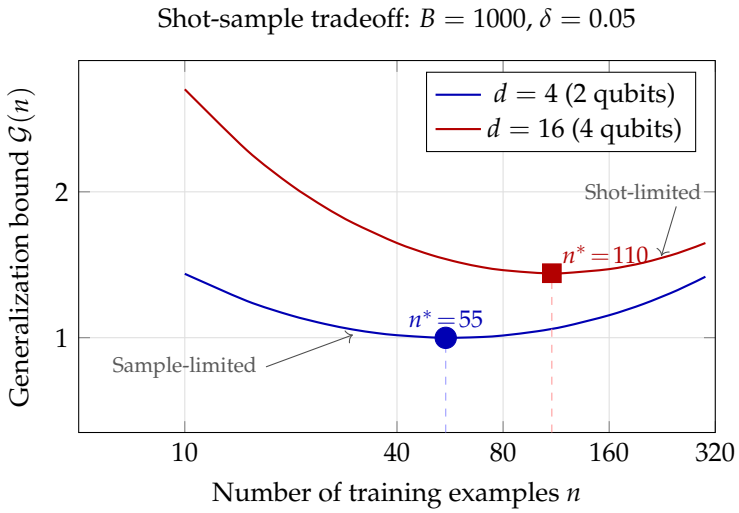

Figure 2: Shot-sample tradeoff for $B = 1000$ and $\delta = 0.05$. The dashed vertical lines show the surrogate allocations $n^* = 55$ for $d = 4$ and $n^* = 110$ for $d = 16$. The exact minimizers of the original logarithmic objective can be computed numerically; the surrogate allocations are used here because they give a closed-form planning rule with the same asymptotic scaling. To the left of the allocation, the bound is mainly sample-limited, so increasing the number of training states is beneficial. To the right, the bound becomes shot-limited, as each state receives too few measurements for accurate score estimation.

To obtain a closed-form allocation rule, we replace $\log(2n/\delta)$ by $\log(2B/\delta)$ in (10), yielding a conservative surrogate objective $\mathcal{G}_C(n) = 2\sqrt{d}/\sqrt{n} + \sqrt{n\log(2B/\delta)/(2B)}$ that has the same asymptotic scaling in B as the original. This substitution is a conservative upper bound on the original objective for $n \le B$ (since $\log(2n/\delta) \le \log(2B/\delta)$ whenever $n \le B$), so the allocation derived from $\mathcal{G}_C$ remains a valid, if conservative, planning rule for the original bound. The surrogate is used for interpretability and closed-form planning; the exact minimiser of the original logarithmic objective satisfies the implicit equation

$$n\big(\log(2n/\delta) + 1\big) = 2\sqrt{2dB\log(2n/\delta)},$$

which can be solved numerically when high precision is required. The resulting closed-form surrogate allocation is stated in Appendix C.

Theorem 3.2. Conservative surrogate allocation rule

Under total budget $B = n \times S$, the allocation minimising the conservative surrogate $\mathcal{G}_C(n)$ is:

$$n^* = 2\sqrt{\frac{2dB}{\log(2B/\delta)}}, \qquad S^* = \frac{B}{n^*} = \frac{1}{2}\sqrt{\frac{B\log(2B/\delta)}{2d}} \tag{11}$$

Both n^* and S^* scale as $\sqrt{B/\log B}$. At this surrogate allocation:

$$\mathcal{G}_C(n^*) = O\left(\left(\frac{d\log(2B/\delta)}{B}\right)^{1/4}\right)$$

The exact minimiser of the original objective (with $\log(2n/\delta)$ treated as a function of n) satisfies an implicit equation and can be solved numerically; the surrogate n^* above has the same asymptotic scaling and is used here for planning and interpretability.

Table 4 summarises the three operating regimes and the recommended actions; Table 5 provides numerical values for representative budgets.

Table 4: Operating regimes under fixed budget $B = n \times S$.

Regime	**Condition**	**Dominant term**	**Recommended action**
Sample-limited	$n \ll n^*$	$2\sqrt{d/n}$	Increase n, reduce S
Balanced	$n \approx n^*$	Both comparable	Near-optimal; increase B if further reduction needed
Shot-limited	$n \gg n^*$	$\sqrt{n\log n/B}$	Decrease n, increase S

Table 5: Closed-form surrogate allocation and original logarithmic bound values evaluated at the surrogate allocation $(n^\star, S^\star)$, with $\delta = 0.05$. The confidence term is excluded to isolate the dominant shot-sample tradeoff. Here $f_1(n^\star)$ is the sample term and $f_2(n^\star)$ is the original logarithmic shot term using $\log(2n^\star/\delta)$, not the conservative surrogate $\log(2B/\delta)$.

B	d	n^*	S^*	$f_1(n^*)$	$f_2(n^*)$	**Bound**
500	4	40	12	0.632	0.543	1.175
500	16	80	6	0.894	0.804	1.698
1000	4	55	18	0.539	0.460	0.999
1000	16	110	9	0.763	0.679	1.442
5000	4	114	44	0.375	0.310	0.685[†]
5000	16	229	22	0.529	0.457	0.986[†]

[†] Theory-only rows. Empirical consistency checks cover $B \in \{500, 1000, 2000\}$; the $B = 5000$ entries illustrate the asymptotic $B^{-1/4}$ trend and were not included in the simulator experiments.

4 Experimental Consistency Checks

4.1 Objectives and Setup

Two categories of experiment are conducted. First, a **direct numerical check** (Experiment 0) computes the empirical Rademacher complexity of the full $\mathcal{H}_{\mathrm{POVM}}$ class using the spectral formula of Proposition 3.1, verifying that empirical estimates remain below the theoretical bound. Second, **end-to-end VQC experiments** (Experiments 1–4) train variational quantum circuits and check that the empirical one-sided test-train gap remains below the theoretical bound. As VQCs constitute a restricted subclass of $\mathcal{H}_{\mathrm{POVM}}$ on structured synthetic data, these latter experiments serve as empirical consistency checks: they demonstrate non-violation of the bound but should not be interpreted as empirical tightness demonstrations. The bound covers the worst case over all of $\mathcal{H}_{\mathrm{POVM}}$; a VQC subclass on easy structured data is a highly favourable special case and will naturally produce gaps far below the worst-case bound.

Implementation. All experiments are implemented using PennyLane [22] with the `lightning.qubit` simulator. VQCs employ R_Y angle embedding and `BasicEntanglerLayers` with $L = 2$ layers, optimised via gradient descent on the hinge loss. Test evaluation uses $n_{\mathrm{test}} = 500$ and $S_{\mathrm{test}} = 2000$ shots with fixed random seeds.

In the experiments we use the rescaled binary hinge loss

$$\ell_{\mathrm{hinge}}(p, y) = \frac{1}{2} \max\{0, 1 - (2y - 1)(2p - 1)\},$$

which is bounded in $[0, 1]$ and is 1-Lipschitz in p.

The use of finite-shot simulation is motivated by the fact that expectation-value based QNNs can suffer substantial output variance under finite sampling, even before hardware noise is included [23].

Benchmark datasets. Nine two-dimensional synthetic binary classification benchmarks are used: three two-moons variants (`moons_noise005/015/030`), two concentric-circles variants (`circles_factor03/06`), two Gaussian benchmarks (`classification_easy/hard`), and two blob benchmarks (`blobs_tight/spread`).

System configurations. Experiments are conducted for $k = 2$ qubits ($d = 4$) and $k = 4$ qubits ($d = 16$).

Validity metric. Theorem 3.1 is a one-sided upper bound on $R_\ell(M) - \hat{R}_{n,S,\ell}(M)$. The appropriate empirical diagnostic is the one-sided gap:

$$\widehat{\Delta}_+(n, S) = \max\{0,\ \hat{R}_{\mathrm{test}} - \hat{R}_{\mathrm{train}}\}$$

No empirical violation is observed by checking whether $\widehat{\Delta}_+(n, S)$ remains below the bound from Theorem 3.1 in the tested configurations. For the empirical bound diagnostic, the trained circuit is treated as fixed and the reported train/test risk estimates are computed using fresh measurement samples independent of the optimisation trajectory. Accordingly, the VQC experiments are consistent with the theorem scope for the post-training evaluation use case, and should be interpreted as heuristic consistency checks rather than direct tests of the bound for adaptive shot-noisy training.

4.2 Experiment 0: Direct Rademacher Complexity Check

For $d \in \{4, 8, 16\}$ and $n \in \{10, 20, 40, 80, 160, 320\}$, the empirical Rademacher complexity is computed via the spectral formula: for each random sign vector σ, the supremum is attained by summing the positive eigenvalues of the signed-average matrix $A_\sigma = \frac{1}{n} \sum_i \sigma_i \rho_i$.

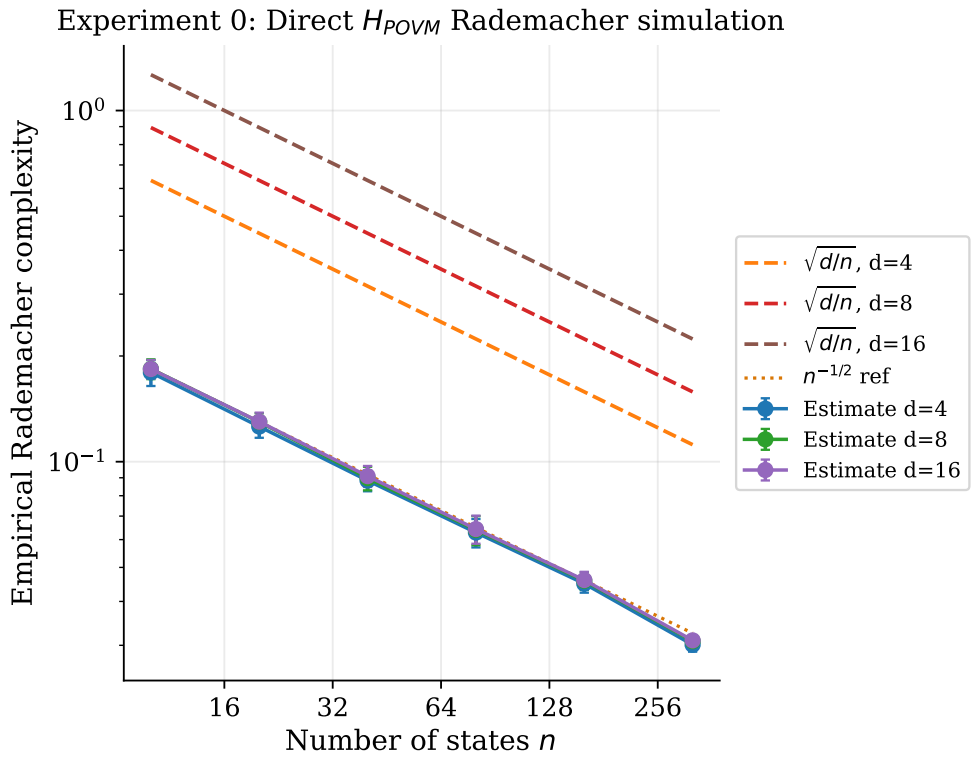

Figure 3: Experiment 0. Empirical Rademacher complexity of the full $\mathcal{H}_{\text{POVM}}$ class as a function of n. Dashed curves: $\sqrt{d/n}$ upper bound. Solid curves: empirical estimates (mean $\pm$ standard deviation over random sign vectors). All estimates remain below the theoretical bound and follow the predicted $n^{-1/2}$ decay.

Finding. The empirical estimates remain below the theoretical bound $\sqrt{d/n}$ for all tested (d, n) configurations. This provides a direct numerical consistency check of Proposition 3.1.

4.3 Experiment 1: Varying Number of Training States

The number of shots is fixed at $S = 100$. The number of training states n is swept over $\{10, 20, 40, 80, 160\}$ for $d \in \{4, 16\}$ across all nine benchmark datasets.

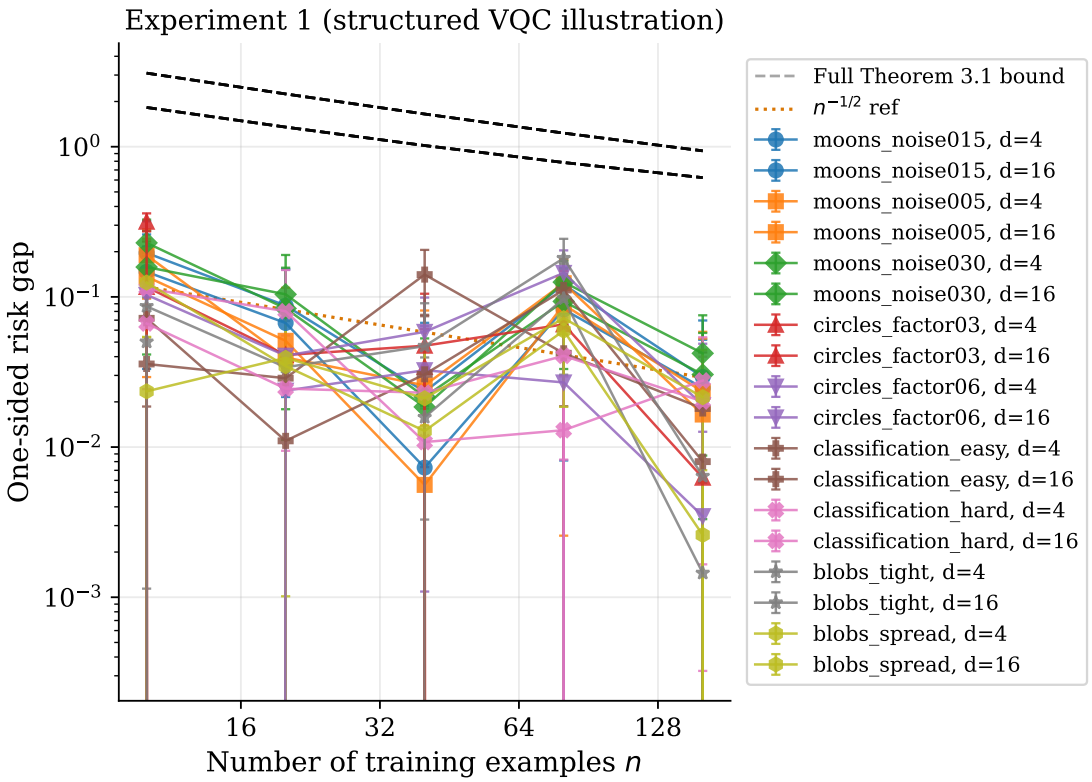

Figure 4: Experiment 1. One-sided empirical generalization gap as a function of n. Black dashed line: Theorem 3.1 bound. Dotted line: $n^{-1/2}$ reference slope. All empirical gaps remain below the theoretical bound across all benchmarks and system sizes.

Table 6: Experiment 1: aggregate log-log slope of the one-sided risk gap as a function of n. Reference slope predicted by theory: $-1/2$.

d	Datasets	Mean slope	Std. (across datasets)
4	9	-0.607	0.371
16	9	-1.216	1.365

Theoretical reference slope: -0.5.

Finding. The non-violation condition is satisfied throughout. For $d = 4$, the empirical log-log slope (-0.607) is broadly consistent with the theoretical prediction of -0.5. For $d = 16$, the slope exhibits greater variance, as empirical gaps are near-zero and VQC optimisation variance is the dominant contributor; this case provides a qualitative consistency check only.

4.4 Experiment 2: Varying Shots Per Training State

The number of training states is fixed at $n = 80$. The shots per state S is swept over $\{10, 25, 50, 100, 250, 500\}$ for $d \in \{4, 16\}$.

Finding. The theoretical bound is not violated for any tested value of S. The approximate flatness of empirical gaps, rather than the $S^{-1/2}$ decay of the shot term, is consistent with the VQCs being sample-limited at $n = 80$.

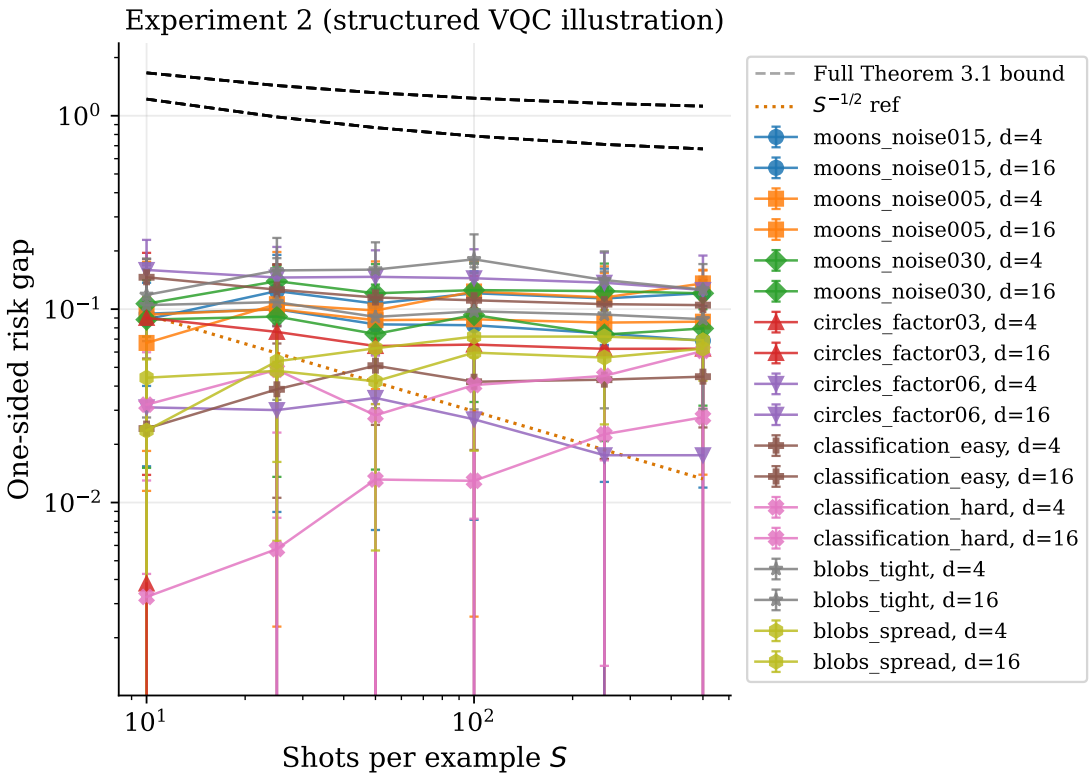

Figure 5: Experiment 2. One-sided empirical gap as a function of S. The theoretical shot term decays as $S^{-1/2}$. Empirical VQC gaps are approximately flat because the tested configurations lie within the sample-limited regime at $n = 80$, where the shot term is not the dominant error source.

4.5 Experiment 3: Fixed Total Budget

The total budget B is fixed at each value in $\{500, 1000, 2000\}$. For each (B, d) pair, the number of training states n is swept on a logarithmic grid with $S = \lfloor B/n \rfloor \geq 5$.

Finding. The theoretical bound is not violated in any configuration. The U-shaped tradeoff predicted by the analysis is clearly visible in the bound curves. The empirical VQC gaps are too flat to precisely locate the empirical minimum, as the structured synthetic tasks do not produce sufficiently large gaps; this is consistent with the bound being conservative for this restricted subclass.

4.6 Experiment 4: Bound-to-Gap Ratios

Finding. Bound-to-gap ratios range from $94\times$ to $463\times$. This degree of conservatism is consistent with the bound being a distribution-free worst-case guarantee over all of $\mathcal{H}_{\text{POVM}}$, whereas the VQC experiments employ a restricted subclass on structured synthetic benchmarks where generalization is inherently easier. The slack is strictly positive in every configuration, confirming non-violation in all cases. These results are consistent with the theoretical bound but should not be interpreted as empirical confirmation of the $B^{-1/4}$ rate or as evidence of bound tightness.

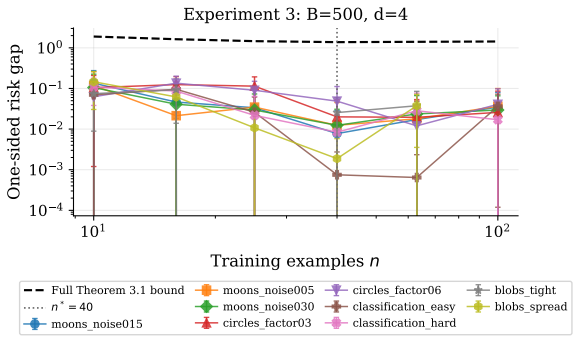

(a) $B = 500$, $d = 4$

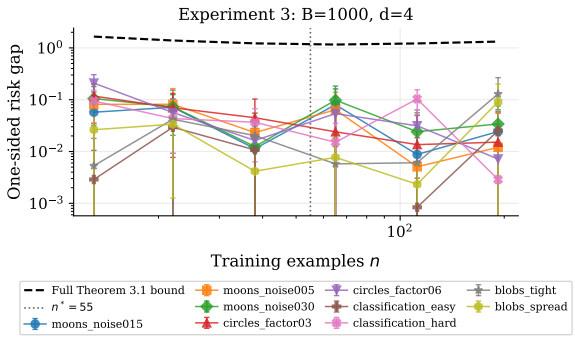

(b) $B = 1000$, $d = 4$

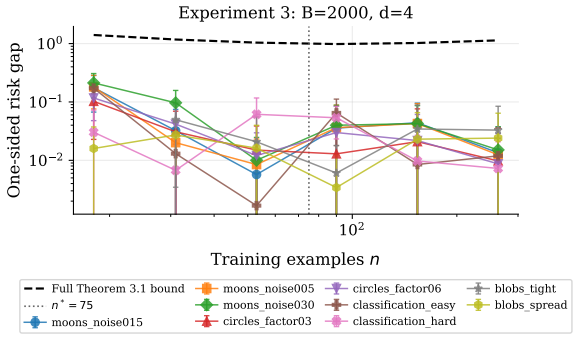

(c) $B = 2000$, $d = 4$

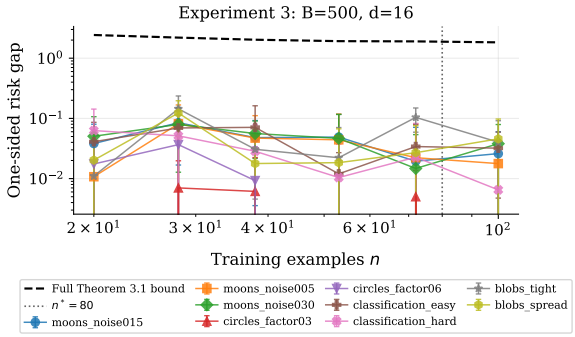

(d) $B = 500$, $d = 16$

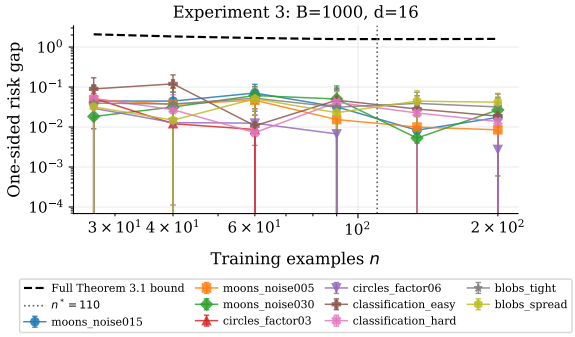

(e) $B = 1000$, $d = 16$

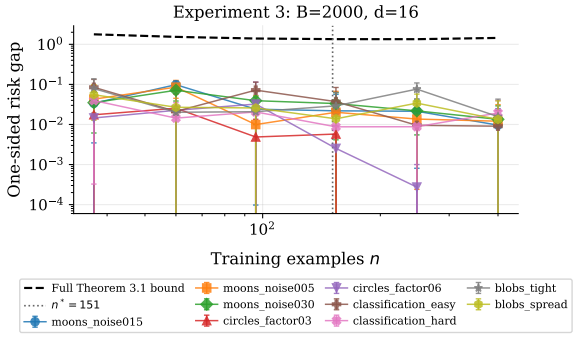

(f) $B = 2000$, $d = 16$

Figure 6: Experiment 3. One-sided empirical gap under fixed budget $B = nS$, as a function of n. Coloured curves: empirical VQC gaps across nine benchmark datasets. Black dashed line: Theorem 3.1 bound. Dotted vertical line: closed-form surrogate allocation n^* illustrating the theoretical planning rule rather than a confirmed empirical minimum. The U-shaped tradeoff is clearly visible in the theoretical bound; empirical VQC gaps are approximately flat because the benchmark tasks are insufficiently challenging to stress-test the bound near its minimum.

Table 7: Bound-to-gap ratios at the predicted allocation (n^*, S^*), averaged over all nine benchmark datasets. Entries with $\widehat{\Delta}_+ < 10^{-3}$ are excluded as numerically unreliable. Large ratios are expected and consistent with the bound being a distribution-free worst-case guarantee over all of $\mathcal{H}_{\mathrm{POVM}}$, while the VQC subclass on structured synthetic data represents a highly favourable special case. Non-violation of the bound (slack > 0 in all cases) is the primary validity criterion; the ratios quantify the degree of conservatism.

B	d	n^*	S^*	Bound	Gap	Slack	Ratio / reported
500	4	40	12	1.427	0.0203	1.4118	94.15 / 9/9
500	16	80	6	1.901	0.0102	1.8917	268.40 / 9/9
1000	4	55	18	1.205	0.0162	1.1926	128.44 / 9/9
1000	16	110	9	1.603	0.0063	1.5963	329.41 / 8/9
2000	4	75	26	1.028	0.0096	1.0209	181.22 / 9/9
2000	16	151	13	1.363	0.0052	1.3576	463.29 / 9/9

5 Discussion

5.1 Interpretation of the $B^{-1/4}$ Rate

The $B^{-1/4}$ rate at the surrogate allocation is slower than the classical $O(B^{-1/2})$. This is a structural consequence of the two-resource budget constraint and does not indicate that quantum learning is intrinsically less efficient than classical learning.

Remark: The two-resource bottleneck

Classical learning is governed by a single resource (n examples) and one error term ($O(1/\sqrt{n})$). The optimal rate is $B^{-1/2}$.
Quantum learning under a finite measurement budget B is governed by two resources (n training states, S shots per state) and two error terms that trade off. The surrogate joint optimum balances both at rate $O(B^{-1/4})$.
The comparison is meaningful only when B is measured in the same units. In the quantum setting, B counts individual binary measurement outcomes, which are a finer unit than a classical training example. At the level of independent experimental runs—one quantum experiment $=$ $(\rho_i, S\text{-shots})$ $=$ one classical example—the two rates are directly comparable.

5.2 Implications for Quantum-Technology Resource Planning

The surrogate allocation formula (n^*, S^*) provides a principled statistical starting point for designing quantum learning experiments on near-term devices. Its practical use can be summarised as follows.

How to apply the surrogate allocation rule. Given a total measurement budget B (e.g., a fixed number of circuit executions on a cloud quantum platform), qubit count k, and confidence parameter δ, compute:

$$n^* = 2\sqrt{\frac{2 \cdot 2^k \cdot B}{\log(2B/\delta)}}, \qquad S^* = \frac{B}{n^*}$$

Collect n^* distinct training states and devote S^* shots to each. This allocation minimises the conservative surrogate planning bound derived from Theorem 3.1; the exact minimizer of the original objective can be found numerically.

Sample-limited regime. If the current experimental configuration has $n \ll n^*$ (few training states relative to the budget), the dominant source of generalization error is the finite-sample term $2\sqrt{d/n}$. Reallocating budget from shots to training states—reducing S and increasing n—will improve the worst-case bound. This regime is common in practice, as large S is conventional in QML.

Shot-limited regime. If the current configuration has $n \gg n^*$ (many training states relative to the budget), the dominant source of error is the shot term $\sqrt{n \log n / B}$. Reallocating toward fewer training states with more shots each will improve the bound.

Relevance to cloud quantum devices and queue-limited experiments. On cloud quantum platforms, circuit executions are metered, queued, and subject to device availability. The allocation formula provides a principled basis for partitioning a fixed execution quota. For queue-limited experiments where additional states can be prepared more easily than additional

shots can be executed (or vice versa), the regime characterisation in Table 4 identifies which resource is the current bottleneck and which adjustment is warranted.

Relevance to quantum simulator studies. On classical simulators of quantum circuits (as used in the present experiments), shots are cheaper but still consume computation time. The allocation formula provides the same guidance: simulator studies that use very large S and small n may be operating in the sample-limited regime and could obtain better worst-case guarantees by redistributing their simulation budget.

Scope of the surrogate formula. The surrogate allocation formula (n^*, S^*) is a *statistical planning rule*, not a hardware scheduler. It does not account for gate errors, decoherence, readout errors, or queue constraints. Incorporating these factors into the allocation framework is identified as future work. On current NISQ devices, hardware noise imposes a noise floor on top of the statistical shot term; the formula should be regarded as an idealized lower bound on the required shot count, to be adjusted upward based on device-specific noise characterisation.

This distinction is important because hardware noise can impose limitations that are qualitatively different from statistical shot noise, including readout errors, gate noise, decoherence, and noise-induced trainability effects in variational algorithms [2, 24].

5.3 Limitations

L1. Conservative bound. The bound is distribution-free and therefore conservative. It covers the worst case over the full class $\mathcal{H}_{\mathrm{POVM}}$, all distributions $\mathcal{P}$, and all training sets of size n. For structured subclasses (e.g., Pauli measurements, shallow PQCs) on structured data distributions, the effective complexity may be substantially smaller than $\sqrt{d/n}$, and the bound will overestimate the true generalization gap. This conservatism is an inherent feature of distribution-free worst-case analysis.

L2. No hardware noise model. The current analysis isolates statistical shot noise and does not model hardware noise, readout error, gate error, decoherence, or calibration drift. On physical NISQ devices, these mechanisms impose additional noise floors that are not captured by the shot term. Incorporating hardware noise into the allocation framework is essential before the formula can serve as a practical guide for physical quantum experiments, and is identified as important future work.

L3. Fixed measurement operator. The theorem requires M to be selected independently of the shot outcomes used to form $\hat{R}_{n,S,\ell}(M)$. This covers resource planning and post-training evaluation but does not directly cover adaptive training procedures in which M is iteratively updated using the same shot-noisy empirical losses. Extending the result to fully adaptive, shot-noisy training algorithms requires additional uniform convergence or algorithm-specific arguments.

L4. Restricted hypothesis class in experiments. The VQC experiments test consistency of the bound for a restricted subclass of $\mathcal{H}_{\mathrm{POVM}}$ on synthetic structured data. They confirm non-violation but are not designed to test tightness. Experiments designed to probe the bound near its worst-case configurations—e.g., random measurements on high-entropy states—are identified as future work.

L5. Nuclear-to-Frobenius looseness. The step $\|A\|_1 \leq \sqrt{d}\|A\|_F$ in the Rademacher complexity proof is tight only when all singular values are equal. For low-rank or structured signed-average matrices, the effective dimension may be substantially smaller than d. Replacing d with an effective rank or a PQC-specific measure is an open problem.

L6. Non-adaptive measurement model. The analysis assumes measurement bases are selected independently of previous outcomes (i.i.d. shot model). Adaptive measurement strategies—where the measurement basis is updated based on previous outcomes—may reduce the shot term below the Hoeffding bound. Whether adaptivity can recover the classical $B^{-1/2}$ rate, and whether the no-cloning theorem imposes a fundamental barrier, is an open question.

5.4 Open Problems

OP1. Establish minimax lower bounds for $\hat{\mathcal{R}}_n^{(\infty)}(\mathcal{H}_{\mathrm{POVM}})$ using quantum Fano-type arguments; determine whether $\sqrt{d/n}$ is tight.

OP2. Derive Rademacher complexity bounds for PQC-induced hypothesis classes via the Lipschitz structure of the parameter-shift rule, targeting bounds of order $O(\Lambda L/\sqrt{n})$ that are independent of d.

OP3. Extend the allocation analysis to incorporate hardware noise models (decoherence, readout error) and determine how the surrogate planning allocation shifts in the presence of a noise floor.

OP4. Determine whether adaptive measurement strategies can improve the $B^{-1/4}$ rate, and whether the no-cloning theorem imposes a fundamental information-theoretic barrier.

OP5. Extend the result to adaptive, shot-noisy training procedures using uniform convergence or algorithm-dependent arguments.

OP6. Extend the bounds to quantum covariate shift under channel-induced state drift.

OP7. Generalise the Rademacher analysis to multi-outcome POVMs and observable regression tasks.

OP8. Formalise the connection between the signed-average matrix $\bar{\rho}_\sigma$ and classical shadow tomography estimators.

6 Conclusion

This study addresses a practical design question for quantum learning experiments: given a finite total measurement budget B on a quantum device or simulator, how should it be allocated between the number of distinct training states n and the number of shots S per state?

The main theoretical result is a distribution-free generalization bound for quantum classifiers (Theorem 3.1) that simultaneously accounts for both statistical resources. The bound decomposes into a classical sample term $O(\sqrt{d/n})$ and a quantum-native shot term $O(\sqrt{(\log n)/S})$. Neither term can be derived from the other, and classical learning theory provides no analogue of the shot term. Minimising a conservative closed-form surrogate of the bound over n under the constraint $B = nS$ yields the allocation rule $n^* = 2\sqrt{2dB/\log(2B/\delta)}$, $S^* = B/n^*$, with the worst-case surrogate bound decaying at rate $O(B^{-1/4})$ at the surrogate optimum.

The bound is conservative, as is expected for a distribution-free worst-case result covering the full class $\mathcal{H}_{\mathrm{POVM}}$. Empirical consistency checks using PennyLane on 2-qubit and 4-qubit variational quantum circuits across nine synthetic classification benchmarks show that all

one-sided empirical generalization gaps remain below the theoretical bound in every tested configuration of n, S, and B; no violation is observed.

The practical guidance the result offers is as follows. A *sample-limited* configuration (few training states, many shots per state) should reallocate budget toward additional training states. A *shot-limited* configuration (many states, few shots each) should do the opposite. The surrogate allocation prescribes $n^* \propto \sqrt{B/\log B}$ training states, each measured $S^* \propto \sqrt{B \log B}$ times.

The guarantee applies to fixed or independently selected measurement hypotheses, including post-training evaluation with fresh shots; it does not provide a complete generalization guarantee for fully adaptive shot-noisy training.

Future directions include incorporating hardware noise models (decoherence, readout and gate errors) into the allocation framework, extending the result to adaptive shot-noisy training procedures, deriving tighter effective-dimension bounds for PQC-induced hypothesis subclasses, and validating the allocation principle on physical quantum devices.

References

[1] John Preskill. Quantum computing in the nisq era and beyond. *Quantum*, 2:79, 2018.

[2] Kishor Bharti, Alba Cervera-Lierta, Thi Ha Kyaw, Tobias Haug, Sumner Alperin-Lea, Abhinav Anand, Matthias Degroote, Hermanni Heimonen, Jakob S. Kottmann, Tim Menke, Wai-Keong Mok, Sukin Sim, Leong-Chuan Kwek, and Alán Aspuru-Guzik. Noisy intermediate-scale quantum algorithms. *Rev. Mod. Phys.*, 94:015004, Feb 2022. doi: 10.1103/RevModPhys.94.015004. URL https://link.aps.org/doi/10.1103/RevModPhys.94.015004.

[3] Marco Cerezo, Andrew Arrasmith, Ryan Babbush, Simon C Benjamin, Suguru Endo, Keisuke Fujii, Jarrod R McClean, Kosuke Mitarai, Xiao Yuan, Lukasz Cincio, et al. Variational quantum algorithms. *Nature Reviews Physics*, 3(9):625–644, 2021.

[4] David A. Kreplin and Marco Roth. Reduction of finite sampling noise in quantum neural networks. *Quantum*, 8:1385, June 2024. ISSN 2521-327X. doi: 10.22331/q-2024-06-25-1385. URL https://doi.org/10.22331/q-2024-06-25-1385.

[5] Fangjun Hu and Xun Gao. Generalization Error in Quantum Machine Learning in the Presence of Sampling Noise. *arXiv e-prints*, art. arXiv:2410.14654, October 2024. doi: 10.48550/arXiv.2410.14654.

[6] Jacob Biamonte, Peter Wittek, Nicola Pancotti, Patrick Rebentrost, Nathan Wiebe, and Seth Lloyd. Quantum machine learning. *Nature*, 549(7671):195–202, 2017.

[7] Maria Schuld and Francesco Petruccione. *Supervised Learning with Quantum Computers*. Springer, 2018.

[8] Jonas M. Kübler, Andrew Arrasmith, Lukasz Cincio, and Patrick J. Coles. An Adaptive Optimizer for Measurement-Frugal Variational Algorithms. *Quantum*, 4:263, May 2020. ISSN 2521-327X. doi: 10.22331/q-2020-05-11-263. URL https://doi.org/10.22331/q-2020-05-11-263.

[9] Andrew Arrasmith, Lukasz Cincio, Rolando D. Somma, and Patrick J. Coles. Operator Sampling for Shot-frugal Optimization in Variational Algorithms. *arXiv e-prints*, art. arXiv:2004.06252, April 2020. doi: 10.48550/arXiv.2004.06252.

[10] Matthias C. Caro, Hsin-Yuan Huang, Marco Cerezo, Kunal Sharma, Andrew Sornborger, Lukasz Cincio, and Patrick J. Coles. Generalization in quantum machine learning from few training data. *Nature Communications*, 13(1):4919, 2022.

[11] Tobias Haug and M.S. Kim. Generalization of quantum machine learning models using quantum Fisher information metric. *Physical Review Letters*, 133(5):050603, 2024.

[12] Peter L. Bartlett and Shahar Mendelson. Rademacher and Gaussian complexities: Risk bounds and structural results. *Journal of Machine Learning Research*, 3:463–482, 2002.

[13] Hsin-Yuan Huang, Richard Kueng, and John Preskill. Information-theoretic bounds on quantum advantage in machine learning. *Physical Review Letters*, 126(19):190505, 2021.

[14] Elies Gil-Fuster, Jens Eisert, and Carlos Bravo-Prieto. Understanding quantum machine learning also requires rethinking generalization. *Nature Communications*, 15(1):2277, 2024.

[15] Nader H. Bshouty and Jeffrey C. Jackson. Learning DNF over the uniform distribution using a quantum example oracle. In *SIAM Journal on Computing*, volume 28, pages 1136–1153, 1998.

[16] Srinivasan Arunachalam and Ronald de Wolf. Guest column: A survey of quantum learning theory. *ACM SIGACT News*, 48(2):41–67, 2017.

[17] Kaifeng Bu, Dax Enshan Koh, Lu Li, Qingxian Luo, and Yaobo Zhang. Statistical complexity of quantum circuits. *Phys. Rev. A*, 105:062431, Jun 2022. doi: 10.1103/PhysRevA.105.062431. URL https://link.aps.org/doi/10.1103/PhysRevA.105.062431.

[18] Kaifeng Bu, Dax Enshan Koh, Lu Li, Qingxian Luo, and Yaobo Zhang. Rademacher complexity of noisy quantum circuits. *arXiv e-prints*, art. arXiv:2103.03139, March 2021. doi: 10.48550/arXiv.2103.03139.

[19] Matthias C. Caro, Elies Gil-Fuster, Johannes Jakob Meyer, Jens Eisert, and Ryan Sweke. Encoding-dependent generalization bounds for parametrized quantum circuits. *Quantum*, 5:582, November 2021. ISSN 2521-327X. doi: 10.22331/q-2021-11-17-582. URL https://doi.org/10.22331/q-2021-11-17-582.

[20] Scott Aaronson. Shadow tomography of quantum states. *SIAM Journal on Computing*, 49(5): STOC18–368–STOC18–394, 2020.

[21] Hsin-Yuan Huang, Richard Kueng, and John Preskill. Predicting many properties of a quantum system from very few measurements. *Nature Physics*, 16(10):1050–1057, 2020.

[22] Ville Bergholm, Josh Izaac, Maria Schuld, Christian Gogolin, M. Sohaib Alam, Shahnawaz Ahmed, Juan Miguel Arrazola, Carsten Blank, Alain Delgado, Soran Jahangiri, et al. PennyLane: Automatic differentiation of hybrid quantum-classical computations. *arXiv preprint arXiv:1811.04968*, 2018.

[23] Tarun Dutta, Alex Jin, Clarence Liu Huihong, José Ignacio Latorre, and Manas Mukherjee. Practicality of training a quantum-classical machine in the noisy intermediate-scale quantum era. *iScience*, 28(8):113058, 2025. ISSN 2589-0042. doi: https://doi.org/10.1016/j.isci.2025.113058. URL https://www.sciencedirect.com/science/article/pii/S2589004225013197.

[24] Samson Wang, Enrico Fontana, Marco Cerezo, Kunal Sharma, Akira Sone, Lukasz Cincio, and Patrick J Coles. Noise-induced barren plateaus in variational quantum algorithms. *Nature communications*, 12(1):6961, 2021.

[25] Michel Ledoux and Michel Talagrand. *Probability in Banach Spaces*. Springer, 1991.

Data availability. The synthetic datasets used in this study are generated using the procedures described in Section 4. The generated data and scripts are available from the author upon reasonable request.

Code availability. The PennyLane-based experimental code supporting the findings of this study is available from the author upon reasonable request.

Competing interests. The author declares no competing interests.

Funding. The author received no specific funding for this work.

AI assistance disclosure. During manuscript preparation, language-editing and drafting assistance tools were used to improve clarity and structure. The author reviewed all content and takes full responsibility for the scientific accuracy, completeness, and integrity of the manuscript. No language model is listed as an author or contributor.

A Proof of Proposition 3.1

Statement. The quantum measurement class $\mathcal{H}_{\mathrm{POVM}}$ cannot correlate with arbitrary ± 1 labels better than $\sqrt{d/n}$ in expectation over the random labelling.

Proposition 1 (restated). $\hat{\mathcal{R}}_n^{(\infty)}(\mathcal{H}_{\mathrm{POVM}}) \leq \sqrt{d/n}$.

Proof. **Step 1: Reduction to a single matrix.** For any fixed sign vector σ and any M, linearity of the trace yields:

$$\frac{1}{n}\sum_{i=1}^{n}\sigma_i \operatorname{Tr}(M\rho_i) = \operatorname{Tr}\left(M \cdot \underbrace{\frac{1}{n}\sum_{i=1}^{n}\sigma_i\rho_i}_{=:\bar{\rho}_\sigma}\right)$$

The signed-average matrix $\bar{\rho}_\sigma$ is Hermitian but not in general positive semidefinite, since $\sigma_i \in \{-1, +1\}$.

Step 2: Inner optimisation. For a fixed Hermitian matrix A, the optimisation $\max_{0\leq M\leq I}\operatorname{Tr}(MA)$ is solved by the projector $\Pi_+(A)$ onto the positive eigenspace of A, corresponding to a greedy eigenvalue threshold. The attained maximum satisfies $\|A\|_{1,+} \leq \|A\|_1$. Therefore:

$$\sup_{M\in\mathcal{H}_{\mathrm{POVM}}} \operatorname{Tr}(M\bar{\rho}_\sigma) \leq \|\bar{\rho}_\sigma\|_1$$

Step 3: Nuclear-to-Frobenius norm inequality. The Cauchy–Schwarz inequality applied to the vector of singular values gives $\|A\|_1 \leq \sqrt{d}\|A\|_F$ for any $d \times d$ matrix (tight when all singular values are equal; potentially loose for low-rank A). Therefore:

$$\|\bar{\rho}_\sigma\|_1 \leq \sqrt{d}\|\bar{\rho}_\sigma\|_F$$

Step 4: Expected Frobenius norm. Each ρ_i satisfies $\|\rho_i\|_F^2 = \operatorname{Tr}(\rho_i^2) \leq 1$. For i.i.d. ± 1 signs: $\mathbb{E}[\sigma_i\sigma_j] = 0$ $(i \neq j)$, $\mathbb{E}[\sigma_i^2] = 1$. Therefore:

$$\mathbb{E}_\sigma\left[\|\bar{\rho}_\sigma\|_F^2\right] = \frac{1}{n^2}\sum_{i=1}^{n}\|\rho_i\|_F^2 \leq \frac{1}{n}$$

Jensen's inequality gives $\mathbb{E}[\|\bar{\rho}_\sigma\|_F] \leq 1/\sqrt{n}$.

Combining:

$$\hat{\mathcal{R}}_n^{(\infty)}(\mathcal{H}_{\mathrm{POVM}}) \leq \mathbb{E}[\|\bar{\rho}_\sigma\|_1] \leq \sqrt{d}\cdot\mathbb{E}[\|\bar{\rho}_\sigma\|_F] \leq \sqrt{d}/\sqrt{n} = \sqrt{d/n}$$

□

B Proof of Theorem 3.1

Proof strategy. Two independent concentration events, one per error source, combined via a union bound.

Theorem 1 (restated). *With probability $\geq 1-\delta$ over the sample and shots:* $R_\ell(M) \leq \hat{R}_{n,S,\ell}(M) + 2L\sqrt{d/n} + L\sqrt{\log(4n/\delta)/(2S)} + \sqrt{\log(2/\delta)/(2n)}$.

Proof. Let $\delta_1, \delta_2 > 0$ with $\delta_1 + \delta_2 = \delta$.

Event $\mathcal{E}_1$: sample generalization (probability $\geq 1 - \delta_1$). The standard Rademacher generalization theorem gives:

$$R_\ell(M) \leq \hat{R}_{n,\ell}(M) + 2\hat{\mathcal{R}}_n(\ell \circ \mathcal{F}_{\mathcal{H}_{\text{POVM}}}) + \sqrt{\log(1/\delta_1)/(2n)}$$

The Rademacher contraction lemma [25] gives:

$$\hat{\mathcal{R}}_n(\ell \circ \mathcal{F}_{\mathcal{H}_{\text{POVM}}}) \leq L \cdot \hat{\mathcal{R}}_n^{(\infty)}(\mathcal{F}_{\mathcal{H}_{\text{POVM}}}) \leq L\sqrt{d/n}$$

On $\mathcal{E}_1$:

$$R_\ell(M) \leq \hat{R}_{n,\ell}(M) + 2L\sqrt{d/n} + \sqrt{\log(1/\delta_1)/(2n)} \tag{12}$$

Event $\mathcal{E}_2$: shot concentration (probability $\geq 1 - \delta_2$). Each $\hat{p}_{M,S}(\rho_i)$ is the sample mean of S i.i.d. Bernoulli$(p_M(\rho_i))$ variables. Hoeffding's inequality and a union bound over $i = 1, \ldots, n$:

$$\max_i |p_M(\rho_i) - \hat{p}_{M,S}(\rho_i)| \leq \sqrt{\log(2n/\delta_2)/(2S)}$$

The Lipschitz property of ℓ transfers this to a loss-level bound:

$$\hat{R}_{n,\ell}(M) \leq \hat{R}_{n,S,\ell}(M) + L\sqrt{\log(2n/\delta_2)/(2S)} \tag{13}$$

Combining. On $\mathcal{E}_1 \cap \mathcal{E}_2$ (probability $\geq 1 - \delta$), substituting (13) into (12) and setting $\delta_1 = \delta_2 = \delta/2$ yields the stated bound. □

C Proof of Theorem 3.2

Setup. The original objective to minimise is $\mathcal{G}(n) = 2\sqrt{d}/\sqrt{n} + \sqrt{n\log(2n/\delta)/(2B)}$ over n with $S = B/n$. Because $\log(2n/\delta)$ depends on n, this objective does not admit a closed-form minimiser. We instead minimise the conservative surrogate $\mathcal{G}_C(n) = 2\sqrt{d}/\sqrt{n} + \sqrt{n\log(2B/\delta)/(2B)}$ obtained by replacing $\log(2n/\delta)$ by $\log(2B/\delta)$. For $n \leq B$, this substitution produces a conservative upper bound on the original objective (since $\log(2n/\delta) \leq \log(2B/\delta)$ when $n \leq B$), so the surrogate minimiser provides a valid conservative allocation for the original problem, with the same asymptotic scaling in B.

Theorem 2 (restated). *The minimiser of the surrogate objective $\mathcal{G}_C(n)$ is $n^* = 2\sqrt{2dB/\log(2B/\delta)}$, and at this allocation $\mathcal{G}_C(n^*) = O\big((d\log(2B/\delta)/B)^{1/4}\big)$. The exact minimiser of the original objective $\mathcal{G}(n)$ satisfies the implicit first-order condition*

$$n\big(\log(2n/\delta) + 1\big) = 2\sqrt{2dB\log(2n/\delta)},$$

and can be determined numerically when high precision is required.

Proof. **Step 1: U-shape of the surrogate.** Let $C_\delta := \log(2B/\delta)$. Then $f_1(n) = 2\sqrt{d/n}$ is strictly decreasing and $f_2(n) = \sqrt{nC_\delta/(2B)}$ is strictly increasing, so $\mathcal{G}_C$ has a unique interior minimum.

Step 2: First-order condition for the surrogate. Write $\mathcal{G}_C(n) = an^{-1/2} + bn^{1/2}$ with $a = 2\sqrt{d}$ and $b = \sqrt{C_\delta/(2B)}$. Setting $\mathcal{G}_C'(n) = 0$:

$$-\tfrac{a}{2}n^{-3/2} + \tfrac{b}{2}n^{-1/2} = 0 \implies n = a/b = 2\sqrt{2dB/C_\delta}$$

Step 3: Evaluation at the surrogate optimum. At $n = n^*$:

$$f_1(n^*) = f_2(n^*) = 2^{1/4}\left(\frac{dC_\delta}{B}\right)^{1/4}, \qquad \mathcal{G}_C(n^*) = 2^{5/4}\left(\frac{dC_\delta}{B}\right)^{1/4}$$

Step 4: Exact first-order condition for the original objective. Differentiating $\mathcal{G}(n) = 2\sqrt{d}/\sqrt{n} + \sqrt{n\log(2n/\delta)/(2B)}$ with respect to n and setting the derivative to zero gives:

$$-\frac{\sqrt{d}}{n^{3/2}} + \frac{1}{2\sqrt{2B}} \cdot \frac{\log(2n/\delta) + 1}{\sqrt{n\log(2n/\delta)}} = 0,$$

which simplifies to

$$n\big(\log(2n/\delta) + 1\big) = 2\sqrt{2dB\log(2n/\delta)}$$

This implicit equation can be solved numerically (e.g., via bisection on $[1, B]$) whenever high precision is desired in practice.

Step 5: Validity of the surrogate as a planning rule. For $n^* \leq B$, which requires $8d/C_\delta \leq B$ (satisfied for all practical parameter ranges), $\mathcal{G}_C(n^*)$ upper-bounds $\mathcal{G}(n^*)$, confirming that the surrogate allocation is conservative with respect to the original bound. □